Stochastic Surface-based Modeling of Compensational Cycles of Distal Turbidite Lobes

Michael J. Pyrcz (mpyrcz@ualberta.ca)
Department of Civil & Environmental Engineering
University of Alberta

Octavian Catuneanu (Octavian Catuneanu (octavian@ualberta.ca)
Department of Earth and Atmospheric Sciences
University of Alberta

Clayton V. Deutsch (cdeutsch@ualberta.ca)
Department of Civil & Environmental Engineering
University of Alberta

Turbidite lobes represent significant exploration targets. Compensational cycles are ubiquitous in distal sand lobes in turbidite systems. Associated features such as mud drapes and normal grading within these cycles may result in geologic barriers and baffles to flow and may have a significant impact on oil and gas production.

Well test, seismic data and well log often provide excellent structural and stratigraphic information, but do not adequately resolve these small-scale features. Analog outcrop studies may provide information about the character of these features. This information should be integrated for improved geologic realism of stochastic reservoir models.

A stochastic surface-based simulation approach is introduced to model compensational cycles within turbidite lobes. This algorithm honors the geometries and interrelationships between the cycles, while also honoring a realistic level of conditioning data. This algorithm is demonstrated within a geostatistical workflow with property models constrained to honor trends based on compensational cycles for improved reservoir models. Integration of this geologic information may result in better models of reservoir response and an improved assessment of uncertainty.

Introduction

The inaccessibility of the subsurface generally results in a high degree of uncertainty. Stochastic models are used to quantify this uncertainty. These models provide a measure of uncertainty in reservoir response through the construction of multiple realizations of reservoir properties such as lithofacies, porosity and permeability. Stochastic models are often cell-based; the model is constructed on a by-cell basis. These models are generally limited to reproduction of two point statistics, the semivariogram, and do not reproduce complicated spatial structures. The desire to construct more geologically realistic stochastic models has led to research in object based and surface based models. Object based or Boolean techniques were pioneered by Haldorsen and others (Haldorsen and Chang, 1986; Haldorsen and Lake, 1984; Stoyen et. al., 1987). Surface based techniques have been introduced recently (Deutsch, Xie and Cullick, 2001, Pyrcz and Deutsch,

1

2003). These models reproduce a wide variety of geologic morphologies, such as those found in turbidite systems.

Turbidite systems represent important exploration targets. There has been a rapid increase in exploration in both convergent and passive margins in the last $20 - 30$ years (Stow and Mayall, 2000). The concept of architectural elements has been recently extended to the turbidite setting. Ghosh and Lowe (1993) constructed an hierarchy of process based architectural elements (see Table 1) and Pickering (1995) presented a scheme focused on internal and external geometry.

Rank	Architectural Elements
1st Order	S1,S2,Ta,Tb,Tc,Td and Te
2nd Order	Single, Sediment Unit / Flow Event
3rd Order	Channel / Lobe Fill
4th Order	Channel / Lobe Complex
5th Order	Multi-story Channel / Lobe Stack
6th Order	Fan Complex

Table 1 – the hierarchy of architectural elements in deep-sea clastics (adapted from Ghosh and Lowe, 1993).

The Ghosh and Lowe (1993) scheme is applied in this paper. Individual homogeneous components are identified as 1st order architectural elements. These may be individual components of the Bouma sequence (T_{A-E}), coarser components (S_{1-3}) and conglomerates (R_{1-3}). The 2nd order architectural elements are composed of a single or collections of 1st order elements that represent individual flow events. 3rd and 4th order architectural elements represent reservoir scale features such as lobes or channel levee systems.

There is a great deal of current research into the internal and external geometries and stacking patterns of architectural elements associated with turbidites (Johnson et al., 2001; Satur et al., 2000; Shanmugam, G., 2000; Stow and Johansson, 2000; Stow and Mayall, 2000). Stochastic methodologies are required that reproduce architectural elements while accounting for the inherent uncertainty. A novel approach based on stochastic surface based simulation is introduced to model architectural elements associated with compensational cycles in distal planar lobes. This new algorithm is a generic tool that functions under a variety of facies model assumptions; therefore, it is independent of the recent debate concerning deep-sea clastic terminology, origin and nature (Shanmugan, 2000).

Large Scale Geometries

The large-scale sand bodies in distal deepwater clastics have been characterized as massive sand facies associations (MSFA) by Stow and Johansson (2000) and are classified as 3rd and 4th order architectural elements by Ghosh and Lowe (1993). They include reservoir scale lobes (Stow and Johansson, 2000) and may be correlated in well

log and characterized by seismic survey.   These elements are referred to as lobes in this paper.

Small Scale Geometries

Small-scale geometries are represented 1st and 2nd order architectural elements, individual sediment units (Ghosh and Lowe, 1993). These elements have a thickness of less than a meter to a few meters and are generally below the resolvable limit of seismic, but may impose significant control on the reservoir response (Satur et al., 2000; Slatt et al., 1998). These elements are referred to as flow events in this paper.

Stow and Johansson (2000) noted some important small scale geometric relationships; (**1**) the small scale geometries often mimic the large scale geometry and (**2**) often display a variety of stacking patterns, such as compensational bedding. For example, a lobe may be filled by flow events with similar geometry and compensational cycles (see Figure 1). Compensation cycles are defined as a main characteristic of ancient sandstone lobes (Mutti and Normark, 1987) and are considered virtually ubiquitous in distal lobes (Mutti and Sonnino, 1981). These cycles are illustrated schematically (see Figure 2).

Discussion on Data

Without data there would be little difficulty in reproducing the complicated geometries within a depositional setting. Quantitative dynamic stratigraphy (QDS) models based on initial and boundary conditions and on a continuum of relationships spanning well established fundamental laws, first order approximations, empirical relationships to poorly defined gross empirical relationships are available (Cross and Harbaugh, 1989). These models are able to reproduce the wealth of geometries and relationships observed in the sedimentological record.

While QDS models are useful for refining conceptual models, their chaotic nature renders them unable to be conditional to a realistic level of data. Solving for appropriate initial and boundary conditions to honor conditioning is an intractable inverse problem. Iterative pseudo-inverse modeling approaches are not feasible given the computational requirements of QDS models. This algorithm within a geostatistical workflow allows for conditioning to a variety of conditioning.

Methodology

Reservoir scale lobe geometry is established from the available data. A measurement of uncertainty is assigned based on data accuracy and this uncertainty may be accounted for as simulated fluctuations in the reservoir geometry. The lobe geometry defines the original bathymetry and the reservoir extents.

The algorithm proceeds by generating stochastic flow events characterized by bounding surfaces.   These flow events have geometries based parameter distributions from conditioning and analogue information. The calculation of the stochastic flow events

requires two steps. First, the geometry is generated and then a stochastic residual is added. The geometric construction considers factors such as; (**1**) source location, (**2**) bathymetry, (**3**) flow path and (**4**) characteristic geometry. The stochastic residual accounts for fluctuations within the bounding surfaces and is conditioned to well data.

The source location represents the entry location of a flow event into the lobe. The source is stochastically located along the proximal margin of the lobe prior to each flow event. The source location is drawn from a probability distribution with the probability inversely proportional to the elevation of the margin; therefore, flow events are more likely to enter in the lowest parts of the proximal margin of the lobe. Avulsion does not occur within the lobe (Posamentier and Kolla, in press).

The bathymetry is initialized as the base of the lobe. Subsequent flow events modify this bathymetry, which directly effects path of subsequent flow events. Flow paths are set to follow the path of steepest gradient. The length of the flow path is based on a stochastically drawn lobe size. See Figure 3 for a schematic illustrating the construction of geometry of individual flow events within a lobe.

Nominal amplitude and a variogram model characterize the stochastic residual. The variogram model defines the smoothness of this residual. The residual is simulated by a 2D version of sequential Gaussian simulation (SGSIM) from the geostatistical library (GSLIB from Deutsch and Journel, 1997).

The SGSIM realization is conditioned to neighbouring well data. This process is demonstrated in Figure 4. If the surfaces geometry contradicts data outside a tolerance then the geometry is recalculated. The algorithm terminates when a stochastic surface exceeds the top of the container.

Trends

Reservoir property trend models, constrained to the surface based model of flow events within a reservoir scale lobe, may be calculated. These hierarchical trend models with respect to the flow events and lobes may be incorporated into the stochastic property models. A hierarchical trend model may be calculated by the following steps; (**1**) the trend model is quantified by functions at each scale and in the principal directions relative to the flow axis: *vertical* from the bottom to the top of an architectural element, *longitudinal* from proximal to distal along the primary axis and *transverse* orthogonal from the primary axis to the termination of the architectural element (see Figure 5), (**2**) super position is applied to calculate the trend at each location based on the relative location within each hierarchy of architectural element. Trend multiples are retrieved from the trend functions and are applied as multiplicative factors to the global average (see Equation 1).

$$trend(\mathbf{u}) = \bar{\phi} \cdot V3(\mathbf{u}) \cdot V2(\mathbf{u}) \cdot L2(\mathbf{u}) \cdot L3(\mathbf{u}) \cdot T2(\mathbf{u}) \cdot T3(\mathbf{u}) \tag{1}$$

where $\mathbf{u}$ is a location vector, $\bar{\phi}$ is the global average property and $V3(\mathbf{u})$, $V2(\mathbf{u})$, $L2(\mathbf{u})$, $L3(\mathbf{u})$, $T2(\mathbf{u})$ and $T3(\mathbf{u})$ are the local trend multipliers. This is method of combining the trend multipliers is based on the assumption of conditional independence, and may not be suitable for all settings. The final trend model is standardized to ensure that the global mean is correct and variance or level of variability described by the trend model is appropriate (see Deutsch, 2002; Isaaks and Srivastava, 1989 and Leuangthong and Deutsch, in press, for discussion on the decomposition of trend and residual). Large-scale conditioning from seismic and well test may be integrated by the a posteriori addition of areal and vertical trend into the hierarchical trend model (Pyrcz and Deutsch, 2003).

Demonstration

Multiple surface-based realizations were calculated based on the flow event and lobe geometry shown in Figure 3. The surfaces were conditioned to four wells (see Figure 6). Two realizations are shown in Figure 7. A hierarchical trend model based on the simulated architectural elements was calculated and is shown in Figure 8. The surfaces were loaded into GOCAD^{TM} for visualization. A screen capture of the first ten surfaces is shown in Figure 9, and the same surfaces are shown in Figure 10 with a cut away to expose the stacking pattern of the surfaces. This procedure is demonstrated within a geostatistical workflow with a synthetic, but realistic case study.

Case Study

A synthetic case study was constructed loosely based on Lobe VII of the Cengio Turbidite System, Italy of the Tertiary Piedmont Basin (Cazzolo, Mutti and Vigna, 1985). Lobe VII is dominated by compensational cycles that constrain the distribution of lithofacies. There are many other well studied modern and ancient examples that contain significant compensational cycles including Mississippi Middle Miocene (M4) (De Vray et al.), Gottero Turbidite System, Italy (Nilsen and Abbate, 1985) and Tanqua Karoo Subbasin, South Africa (Dudley et. al, 2000). The Cengio turbidite system is comprised of eight tabular lodes with thickness ranging between five to 25 meters. Lobe VII is roughly 20 meters thick and extends for about six kilometers and is bounded on the west to north by a slope mudstone.

The subsequent flows may be separated by mudstones and have persistent internal lithofacies trends. The mudstone facies are thinly bedded and are not laterally persistent (Cazzolo, Mutti and Vigna, 1985). Even with limited continuity these shales may act as baffles to fluid flow. The modeling of these compensational cycles is an important step in assessing the impact on reservoir response of shale baffles and the other related lithofacies trends.

The Data

The top and bottom of the lobe is correlated in well log and may be below the resolvable limit of seismic. The initial bathymetry will be an approximation of the fault-bounded, southwest-northeast-trending submarine depression (rough approximation of Cazzolo, Mutti and Vigna, 1985, Figure 12).

It is assumed that seven vertical well are available, as indicated in Figure 12. The contacts of the flow events are assumed along the wells with a similar density observed in the Cazzolo, Mutti and Vigna (1985) case study.   Also, porosity and permeability along the wells is assumed. The naïve and declustered data distributions are shown in Figure 13 and the scatter plot of permeability and porosity are shown in Figure 14.   The sections that will be used for visualization are shown Figure 15.

Geostatistical Work Flow

The application of stochastic surface based simulation is demonstrated within a geostatistical workflow for the modeling of petrophysical properties within Lobe VII. A common geostatistical workflow is to model: (**1**) reservoir geometry, (**2**) lithofacies and (**3**) petrophysical properties constrained by lithofacies. These models are conditional to all available data and analogue information (Deutsch, 2002).

Model of Reservoir Geometry

Often reservoir geometry is informed by seismic information calibrated to well log. Seismic resolution is a function of the source frequency content, rock sonic properties and the depth of the trace.   There is commonly a significant level of uncertainty associated with respect to the reservoir geometry. This uncertainty may be carried through the stochastic workflow through the use of multiple reservoir geometry realizations or scenarios.   These scenarios may be the result of simulated surfaces conditioned to well contacts or based of expert judgment of a professional geologists. For this case study a single reservoir geometry was used (see Figure 16).

Lithofacies Models

There are four lithofacies types identified by Cazzolo, Mutti and Vigna (1985). They are summarized below.

Category	Lithofacies	Bedding
Facies 1	sandstone	thick - massive, crudely graded
Facies 2	sandstone	thin - medium
Facies 3	mudstone	thinly bedded sandstone
Facies 4	mudstone	devoid of sandstone

Table 2 – summary of the lithofacies identified by Cazzolo, Mutti and Vigna (1985).

There are significant trends in the facies including: (**1**) higher fraction of sandier amalgamated sandstone bodies along the center axis, (**2**) fining to the distal and (**3**) capping of sandy flows with sandy mudstone (Cazzolo, Mutti and Vigna, 1985). It was decided not to explicitly model lithofacies. Instead porosity and permeability is constrained by trend models that account for these lithofacies trends. This is reasonable since these lithofacies represent a natural continuum from high porosity and permeability sandstone to low porosity and permeability mudstone.

Petrophysical Properties

The petrophysical properties, porosity and permeability, are modeled by the following steps: (**1**) calculate surfaces representing stochastic flow events within the lobe, (**2**) construct a hierarchical trend model that characterizes the observed trends in lithofacies constrained to the surface based model, (**3**) simulate porosity conditional to well log and with the hierarchical trend model as a local variable mean model (Deutsch and Journel, 1997) and (**4**) simulate permeability with the porosity realization as secondary data for collocated cokriging (Deutsch and Journel, 1997).

It is recommended that a single realization of surface-based trend be coupled with a realization of porosity and permeability to produce a single reservoir realization, rather than a combinatorial of matched trend and property realizations. The former is a more computationally efficient method to sample the model space of uncertainty and is applied in this case study (Pyrcz et al., 2003).

This methodology honors the available well log porosity, permeability from log and core, the trend in the porosity and permeability informed by geologic information on the transition in lithofacies, the compensational cycle geometry of the trends in porosity and permeability and the relationship between porosity and permeability. The associated steps are demonstrated and discussed in detail.

The methodology for generating stochastic flow events has been discussed and demonstrated previously. Implementation of this procedure with this specific case study requires; (**1**) the characterization of the lobe geometry and (**2**) the assignment of flow event parameter distributions. The construction of the reservoir geometry has been previously discussed. The flow event parameters were set in an heuristic manner. A

couple test runs were conducted with a variety of parameter distributions to check the manner in which the reservoir geometry is filled. If the distribution of flow event sizes is too small then the distal section of the lobe may not filled. If the distribution of flow event sizes is too large then proximal section of the lobe may fill too rapidly.

For this case study the parameter distributions were drawn from Gaussian and uniform distributions as follows:

$$L \rightarrow N\{5,000,3,000\}$$
$$l \rightarrow U\{0.4 \cdot L, 0.7 \cdot L\}$$
$$W \rightarrow U\{0.1 \cdot L, 0.3 \cdot L\}$$
$$w = 0.4 \cdot W$$

where L is the length of the lobe drawn from a uniform distribution from 3,000 to 6,000 meters, l is the length to the positional of maximum width drawn from a uniform distribution of 10% to 90% of L, W is the maximum lobe width drawn from a uniform distribution of 10% to 50% of L and w is the width at the source assigned as 40% of W.

Two surface based realizations were simulated, based on the reservoir geometry and the distribution of flow event parameters indicated above. The first and second realizations are comprised of 121 and 71 flow events respectively. The long section for two realizations is shown in Figure 17 and the north-south sections for the first realization are shown in and Figure 18.

Each surface based realization honors the identified contacts at the wells. This is demonstrated in Figure 17. Between the wells and at locations along the well missing information the realizations may vary greatly while honoring the flow event geometry and the compensational stacking pattern.

The lithofacies trends were quantified as functions describing the porosity trend in the following. The functions describing these trends are shown in Figure 19. Mud drapes are represented by a sharp decrease in the porosity trend near the top of the flow events and fining towards the peripheries is indicated in the longitudinal and transverse trend functions. The resulting hierarchical trend models based on the two surface based simulations (refer to Figure 17) are shown in Figure 20 and a fence diagram of the first trend model is shown in Figure 21.

These trend models may be applied as local variable mean models for SGSIM (Deutsch and Journel, 1998) of porosity conditioned to well log. SGSIM requires the modeling of semivariograms of the Gaussian transform of the data. The experimental semivariograms were calculated in the plane of the flow events (near horizontal) and orthogonal to the flow events (near vertical). The semivariograms and their associated models are shown in Figure 22. The semivariograms were modeled by a spherical and a Gaussian nested structure.

Two realizations of porosity were calculated each paired with a local variable mean model (refer to Figure 20). These realizations reproduce the porosity conditioning from well log, the declustered porosity distribution and the porosity trends constrained to the stochastic surfaces (see Figure 23 and Figure 24). At the sampled locations along the wells the porosity realizations are the same, but away from the wells the realizations may be quite different, while honoring the local variable trend model and stationary semivariogram.

It is assumed that permeability inferred from log and core is available at the wells (refer to Figure 13). The correlation coefficient between the Gaussian transform of porosity and permeability may be inferred from the available conditioning (refer to Figure 14) and from analogue. The experimental permeability semivariograms were calculated in the plane of the flow events (near horizontal) and orthogonal to the flow events (near vertical). The semivariograms and their associated models are shown in Figure 25.

Two realizations of permeability were simulated with the associated porosity realizations applied as collocated secondary data in a collocated cokriging context (Deutsch and Journel, 1998) (see Figure 26 and Figure 27).

These realizations of reservoir petrophysical properties may be applied for reservoir development planning. These models may be subjected to flow simulation or other transfer functions. For example φh maps may be calculated for each realization (Figure 28).

Limitations

There are a couple limitations with respect to the proposed surface based technique.

- Adequate horizontal discretization is required. If the gradient in the bathymetry is high and the horizontal discretization is course then sharp edges result at the peripheries of the flow events. In the case study with a maximum gradient of one degree a 100 by 100 grid was applied without edge artifacts.

- As the level of conditioning increases or the flow event size increases it is more difficult to match conditioning. This results in more rejected flow event geometries; therefore, great computational effort to calculate realizations. In this example only about twenty percent of geometries were rejected and less than ten minutes was required for each realization.

Summary

- Small-scale features such as compensational cycles may significantly constrain reservoir response and are often below seismic resolution.

- Compensational cycles are common in distal lobes of turbidite systems, which are significant reservoir targets.

- An algorithm for modeling compensational cycles with surface based simulation is proposed that reproduces the geometries and interrelationships of the associated hierarchy of architectural elements.

- The algorithm is demonstrated within a geostatistical workflow for the construction of stochastic models that:

  1. honor the available conditioning data

  2. reproduce trends in petrophysical properties due to compensational cycles

  3. reproduce the relationship between porosity and permeability as characterized by the linear correlation coefficients

- These methodologies may be extended a variety of other depositional systems including deltaic and fluvial.

References Cited

Cazzolo, C, E. Mutti and B. Vigna, 1985, Cengio turbidite system, Italy, in A.H. Bouma, W.R. Normark and N.E. Barnes, eds., Submarine fans and related turbidite systems, New York, Springer-Verlag, p.179-183.

Cross, T.A., and J.W. Harbaugh, 1989, Quantitative dynamic stratigraphy: a workshop, a philosophy, a methodology, in T.A. Cross, eds., Quantitative dynamic stratigraphy, Eaglewood Cliffs, New Jersey, Prentice Hall, p. 3-20.

Deutsch, C. V., 2002, Geostatistical reservoir modeling: New York, Oxford University Press, 376 p.

Deutsch, C.V. and A.G. Journel, 1998, GSLIB: geostatistical software library and users guide: New York, Oxford University Press, 369 p.

Deutsch, C.V., Y. Xie, and A.S. Cullick, 2001, Surface geometry and trend modeling for integration of stratigraphic data in reservoir models: 2001 SPE Western Regional Meeting, March 26-30, Bakersfield, California.

DeVay J.C., D. Risch, E. Scott and C. Thomas, 2000, A Mississippi-sourced, middle Miocene (M4), fine-grained abyssal plain fan complex, northeastern Gulf of Mexico, in A.H. Bouma and C.G. Stone, eds., Fine-grained turbidite systems, AAPG Memoir 72/SEPM Special Publication No. 68, p. 109-118.

Dudley, P.R.C., D.E. Rehmer, and A.H. Bouma, 2000, Reservoir-Scale Characteristics of Fine-Grained Sheet Sands, Tanqua Karoo, South Africa, in P. Weimer et al., eds., Deep-

water reservoirs of the world: GCSSEPM Foundation Proceedings, 20th Annual Research Conference, p. 318 – 342.

Ghosh, B. and D.R. Lowe, 1993, The architecture of deep-water channel complexes, Cretaceous Venado Sandstone Member, Sacramento Valley, California, in Graham, S.A., and Lowe, D.R., eds., Advances in the sedimentary geology of the Great Valley Group, Sacramento Valley, California: Pacific Section, Society of Economic Paleontologists, v. 73, p. 51-65.

Haldorsen, H.H. and D.W. Chang, 1986, Notes on stochastic shales; from outcrop to simulation model, in Lake, L.W. and Caroll, H.B, eds., Reservoir characterization: p. 445-485.

Haldorsen, H.H. and L.W. Lake, 1984, A new approach to shale management in field-scale model, SPE J, p. 447-457.

Isaaks, E.H. and R.M. Srivastava, 1989, An introduction to applied geostatistics: New York, Oxford University Press, p. 561.

Johnson, S.D, F. Stephen, D. Hinds and H.D. Wickens, 2001, Anatomy, geometry and sequence stratigraphy of basin floor to slope turbidite systems, Tanqua Karoo, South Africa: Sedimentology, v. 48, p. 987-1023.

Leuangthong, O. and C.V. Deutsch, in press, Transformation of residual to avoid artifacts in geostatistical modeling with a trend.

Mutti, E. and W.R. Normark, 1987, Comparing examples of modern and ancient turbidite systems: problems and concepts, in J.K. Legget and G.G. Zuffa, eds., Marine clastic sedimentology: concepts and case studies: Graham and Trotman, p. 1-38.

Nilsen, T. and E. Abbate, 1985, Gottero turbidite system, Italy, in A.H. Bouma, W.R. Normark and N.E. Barnes, eds., Submarine fans and related turbidite systems, New York, Springer-Verlag, p. 199-204.

Pickering, K.T., J.D. Clark, R.D.A. Smith, R.N. Hiscott, F. Ricci Lucchi and N.H. Kenyon, 1995, Architectural element analysis of turbidite systems, and selected topical problems for sand-prone deep-water systems, in K.T. Pickering, R.N. Hiscott, N.H. Kenyon, F. Ricci Lucchi, and R.D.A. Smith, eds., Atlas of deepwater environments: architectural style in turbidite systems: London, Chapman, and Hall, p. 1-10.

Posamentier, H.W. and V. Kolla, in press, Seismic geomorphology and stratigraphy of depositional elements in deep-water settings.

Pyrcz, M.J. and C. V. Deutsch, 2003, Stochastic surface modeling in mud rich, fine-grained turbidite lobes: AAPG Annual Meeting, May 11-14, Salt Lake, Utah.

Pyrcz, M.J., E. Gringarten, P. Frykman and C.V. Deutsch, 2003, Representative input parameters for geostatistical simulation, in T.C. Coburn, eds., Stochastic modeling II. AAPG computer applications in geology, No. N.

Satur, N., A. Hurst, B.T. Cronin, G. Kelling and K. Gurbuz, 2000, Sand body geometry in a sand-rich, deep-water clastic system, Miocene Cingoz Formation of Southern Turkey: Marine and Petroleum Geology, v. 17, p. 239-252.

Shanmugam, G., 2000, 50 years of the turbidite paradigm (1950s-1990s): deep-water processes and facies models – a critical perspective: Marine and Petroleum Geology, v. 17, p. 285-342.

Slatt, R.M, G.H. Brown, R.J. Davis, G.R. Clemenceau, J.R. Colbert, R.A. Young, H. Anxionnaz and R.J. Spang, 1998, Outcrop-behind outcrop characterization of thin-bedded turbidites for improved understanding of analog reservoirs: New Zealand and Gulf of Mexico SPE 49563: SPE Annual Technical Conference and Exhibition.

Stow, D.A.V. and M. Johansson, 2000, Deep-water massive sands: nature, origin and hydrocardon implications: Marine and Petroleum Geology, v. 17, p. 145-174.

Stow, D.A.V. and M. Mayall, 2000, Deep-water sedimentary systems: new models for the 21st century: Marine and Petroleum Geology, v. 17, p. 125-135.

Stoyan, D., W.S. Kendall and J. Mecke, 1987, Stochastic Geometry and its applications: New York, John Wiley & Sons, 345 p.
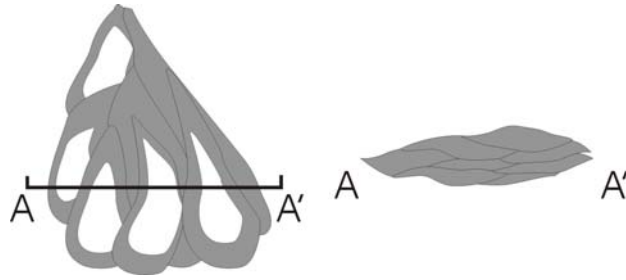
Figure 1 – internal and external geometry of turbidite lobes. The internal geometry is based on flow events with a compensational stacking pattern.
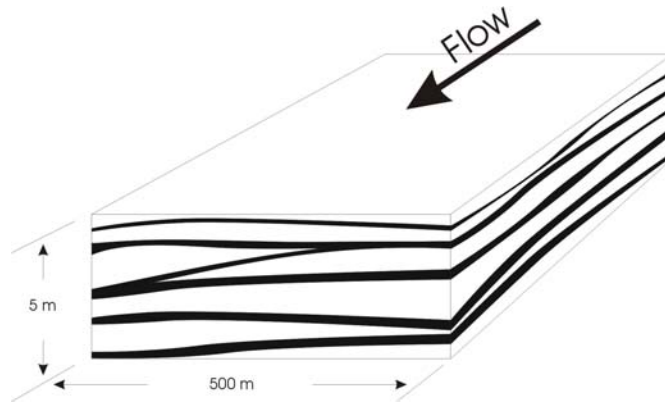
Figure 2 – a drawing similar to the schematic illustration of compensational bedding from Mutti and Sonnino (1981).
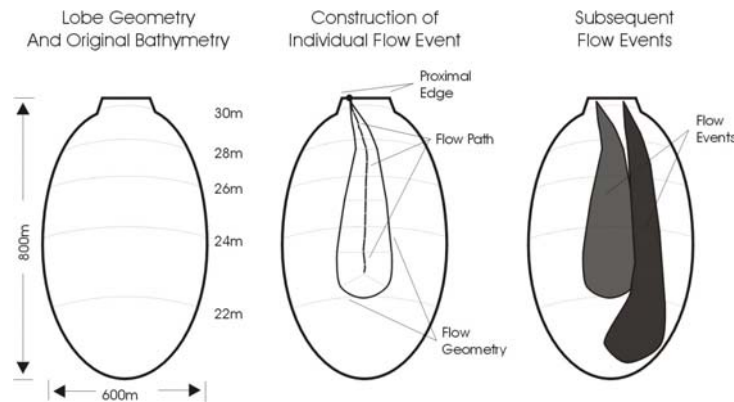
Figure 3 – the construction of individual flow events within a lobe. An example lobe geometry and bathymetry are defined. Stochastic flow events are generated, characterized by flow path and flow geometry.
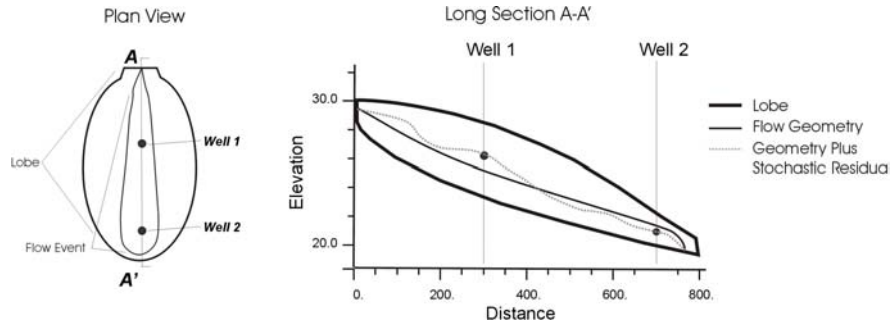
Figure 4 – the addition of a stochastic residual to characterize fluctuations and to allow for conditioning to well data.
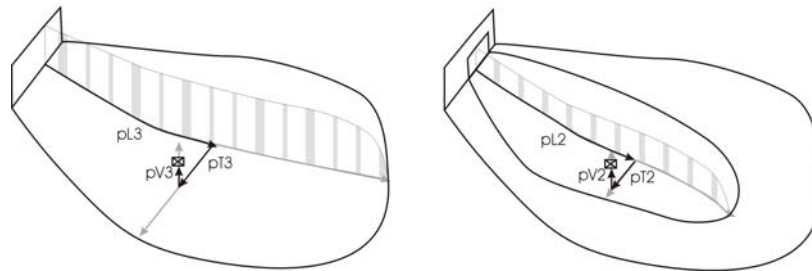
Figure 5 – a demonstration of the coordinate system describing vertical, longitudinal and transverse location within nested architectural elements (left at lobe scale and right at flow event scale). The striped section represents to primary flow axis at each scale.
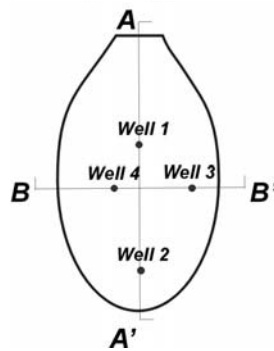
Figure 6 – the lobe geometry, vertical well locations and sections for the demonstration of stochastic surface-based flow events within a lobe.

14
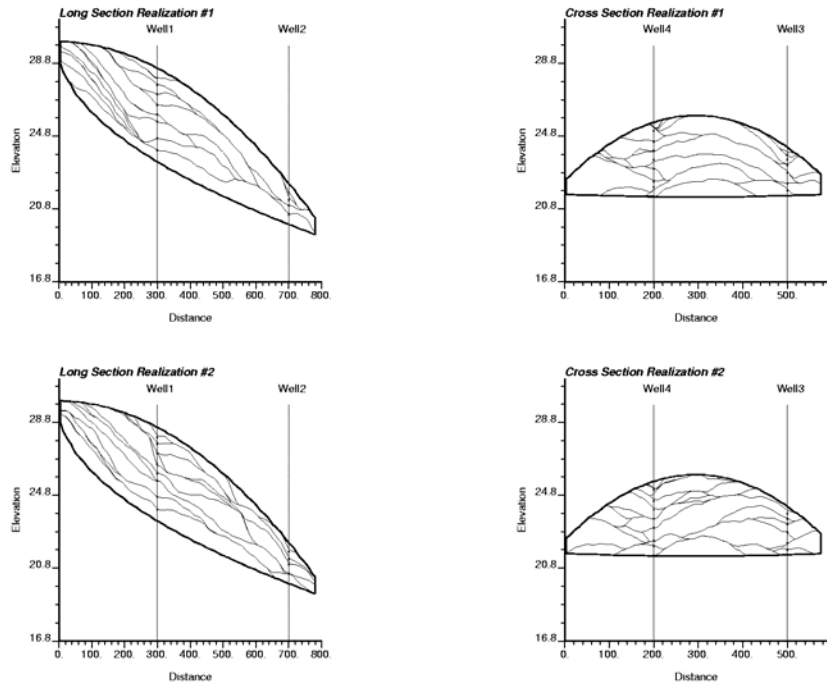
Figure 7 – long and cross sections of two surface-based simulations conditioned to wells.
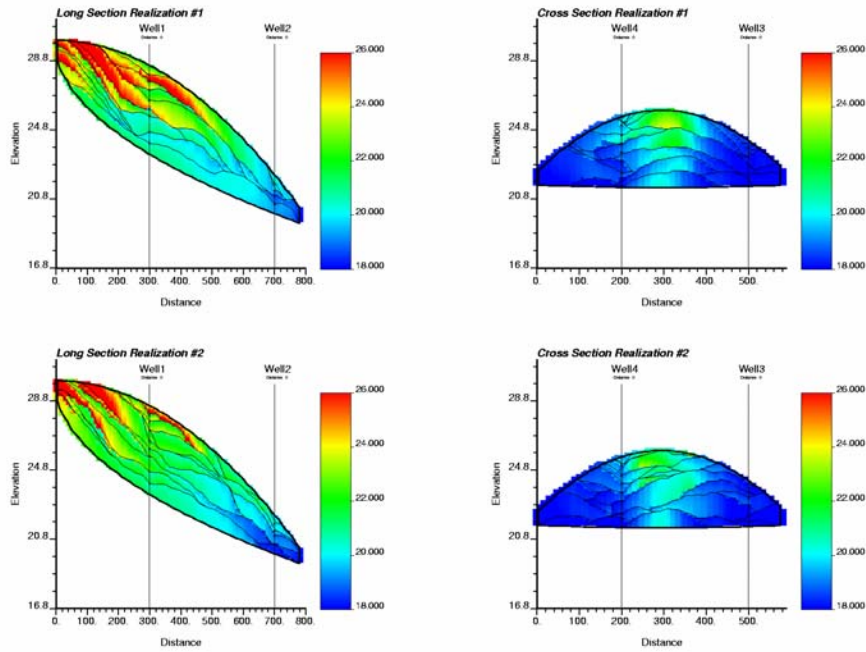
Figure 8 – two example realizations of flow events in a depositional lobe with hierarchical trend models.

15
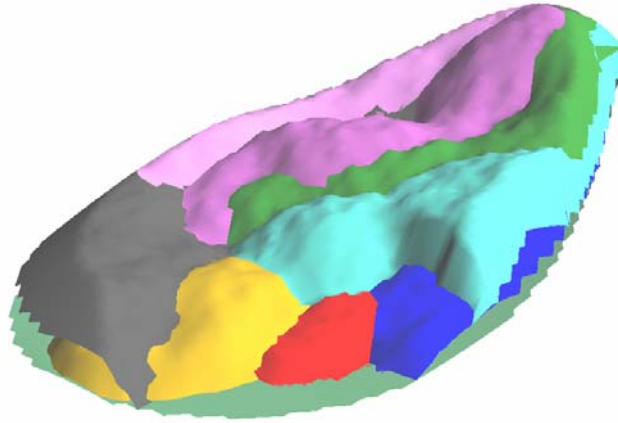
Figure 9 – a screen capture from GOCAD^{TM} of the first ten flow event surfaces.
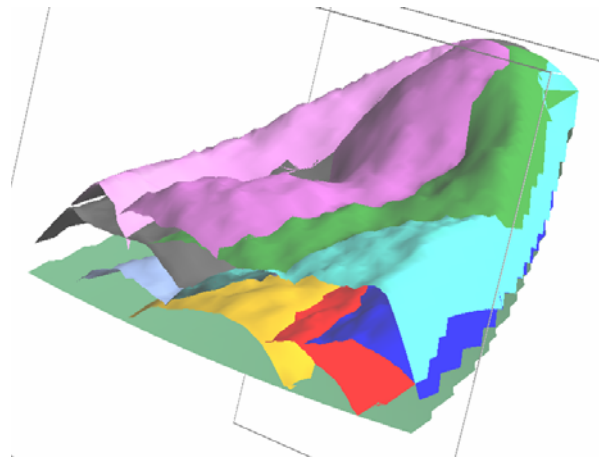
Figure 10 – a screen capture from GOCAD^{TM} of the first ten flow event surfaces with a cut away view to reveal internal structure.
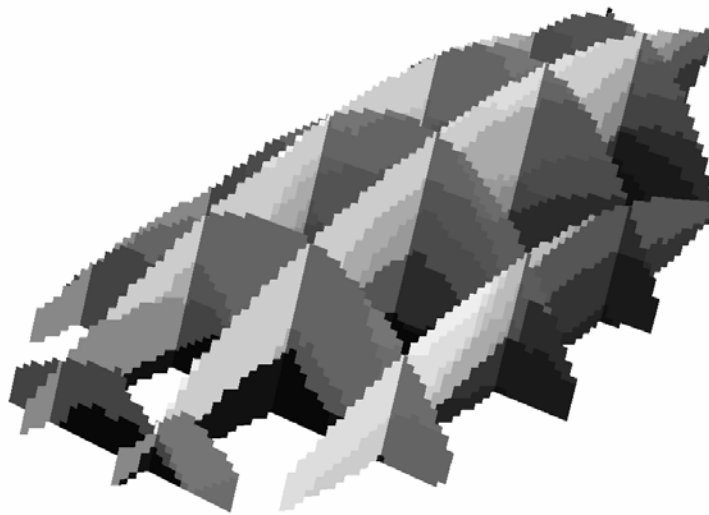
Figure 11 – a fence plot of the discretized architectural element model from GOCAD^{TM}.
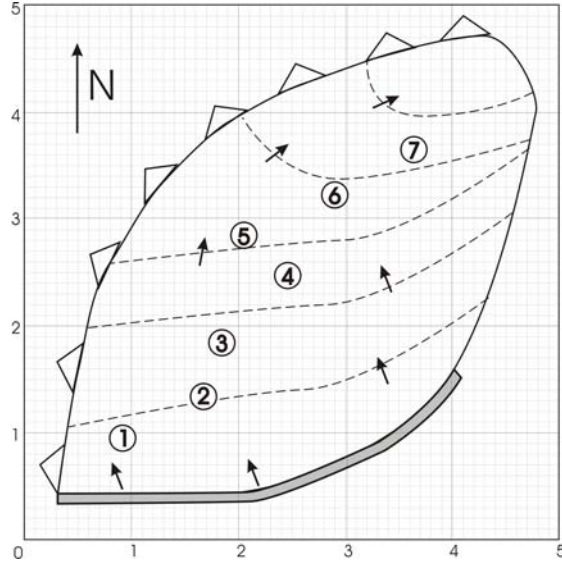
Figure 12 – a schematic of the initial bathymetry loosely based on a study of Cengio turbidite system Italy (Cazzolo, Mutti and Vigna, 1985). The dark gray section represents the source for flow events. The fan lobe onlaps a mudstone slope along the west, northwest and north. The vertical well locations and the paleocurrents are indicated. The study area is 25 square kilometers.
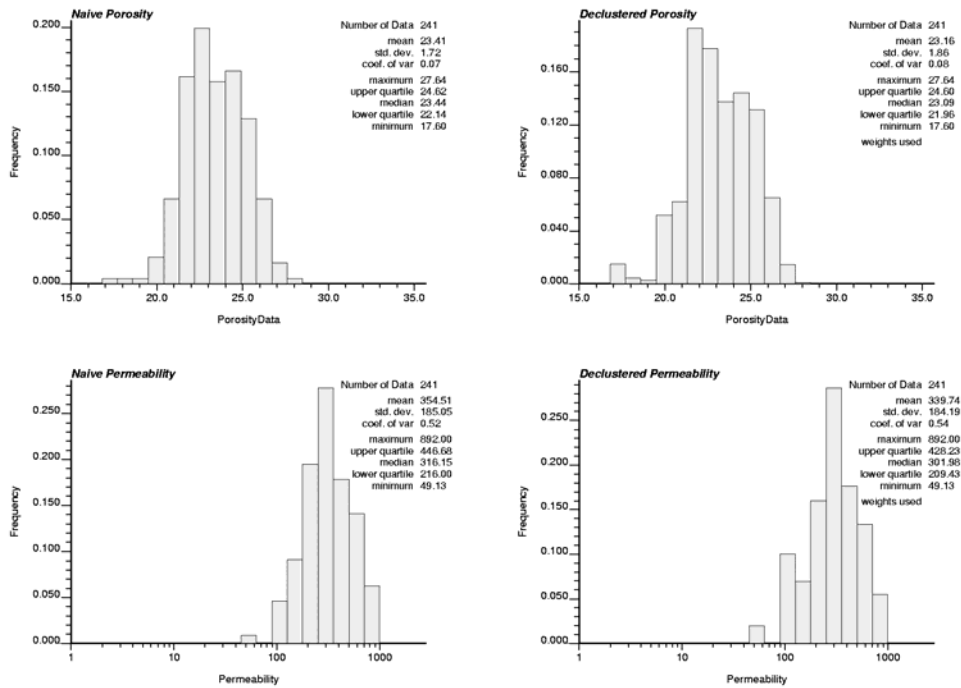
Figure 13 – distribution of porosity and permeability from well log naïve and declustered. Declustering weights are from polygonal declustering within the reservoir geometry.
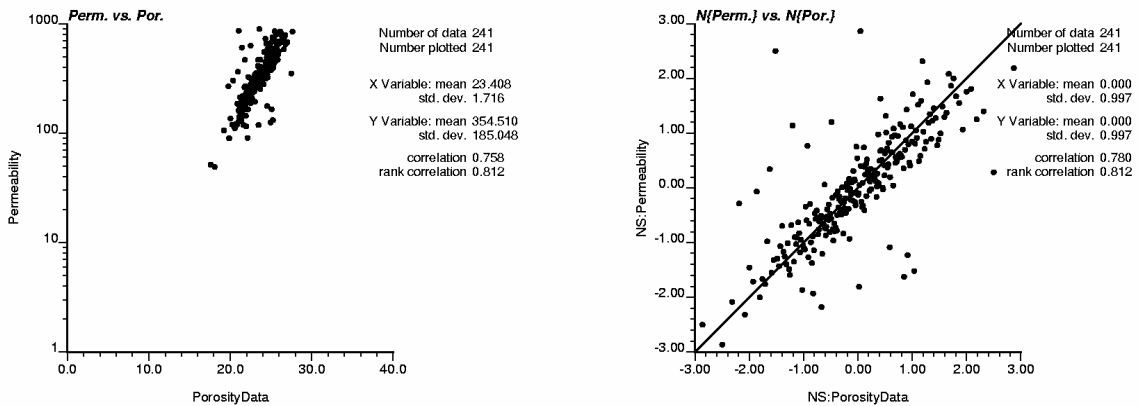
Figure 14 – the scatter plots of well permeability and porosity before and after Gaussian transform. The permeability is in mDarcy and the porosity is in percent.
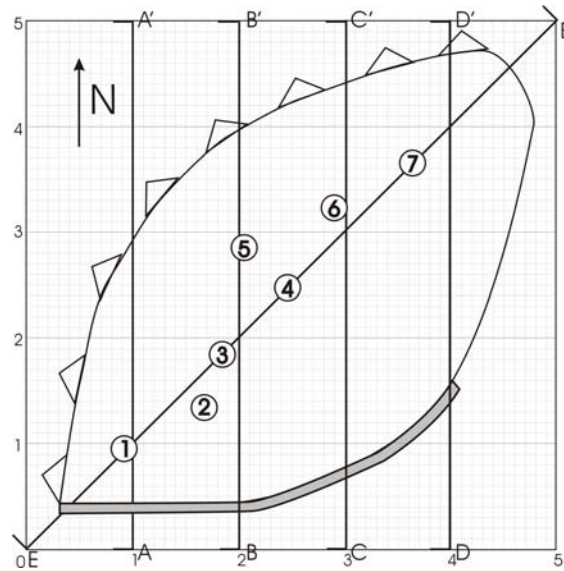
Figure 15 – the locations of the north-south sections (A through D) and the long section (E).
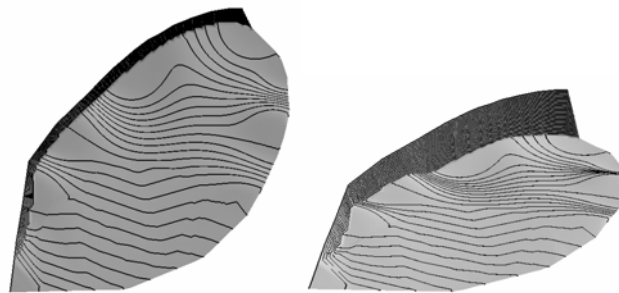
Figure 16 – the inferred bottom bounding surface of Lobe VII of the Cengio Turbidite System, Italy. Left – plan view, north is up, right – oblique view looking north, both with contours every meter.
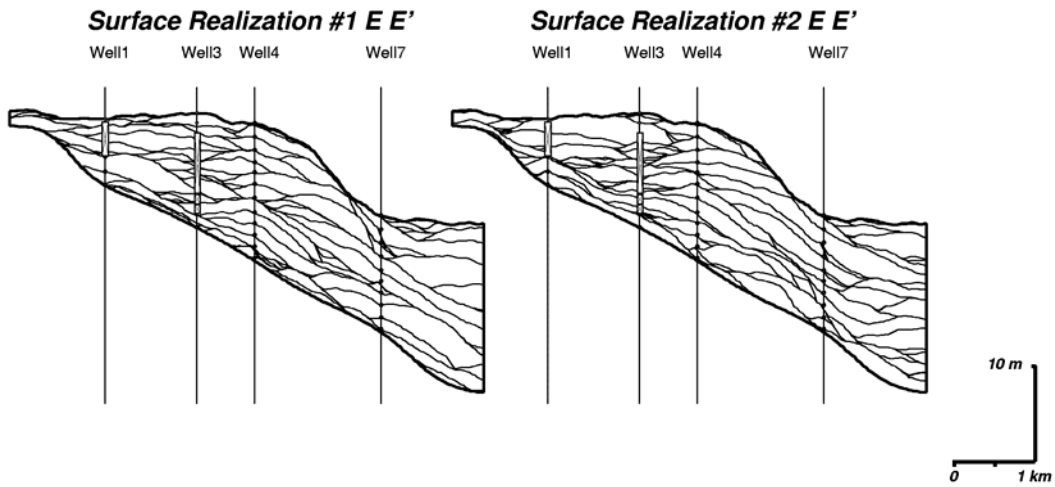
Figure 17 – long section E – E' for two realizations of surfaces.
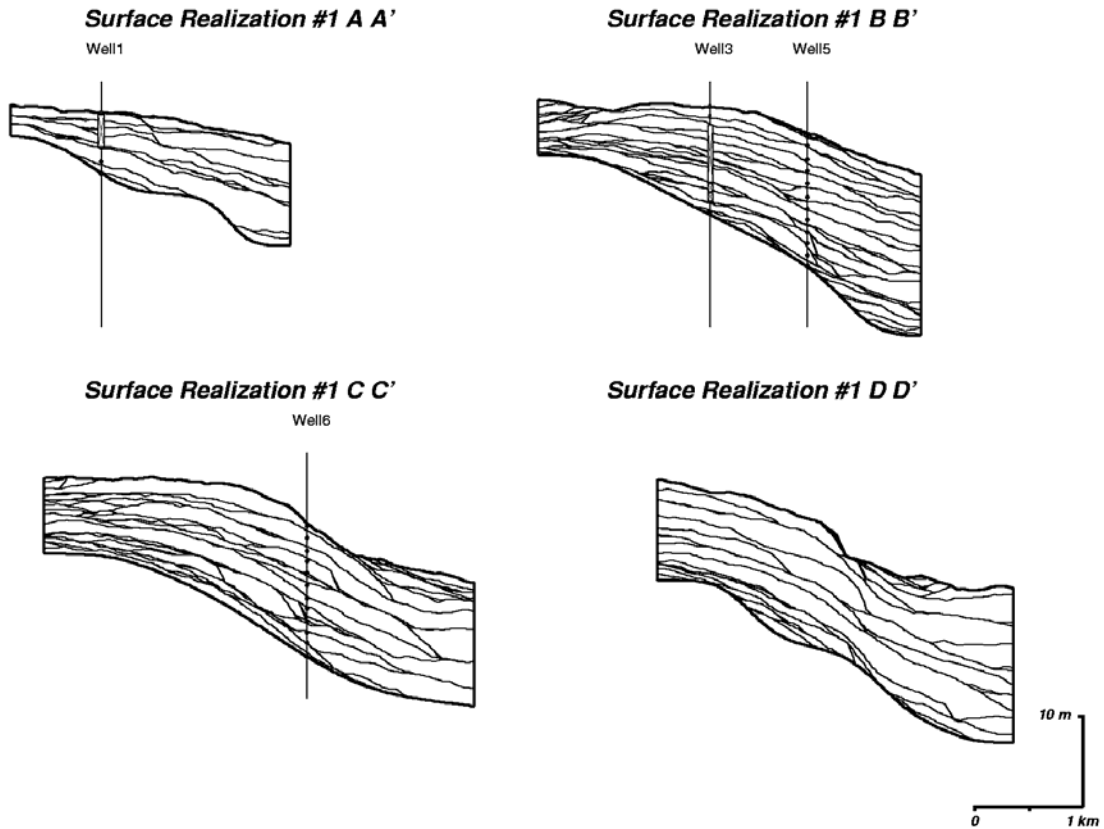
Figure 18 – north-south sections (A through D) for realization one.
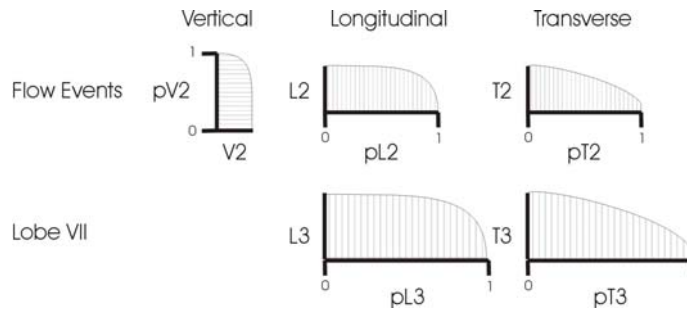
Figure 19 – the porosity trends inferred from the lithofacies study of the Cengio Turbidite System, Italy (Cazzolo, Mutti and Vigna, 1985). The flow events may have subtle grading and are often capped by fine grained facies. Flow events and the lobes demonstrate an increase in fine facies towards the distal and are coarsest along the primary axis of flow.
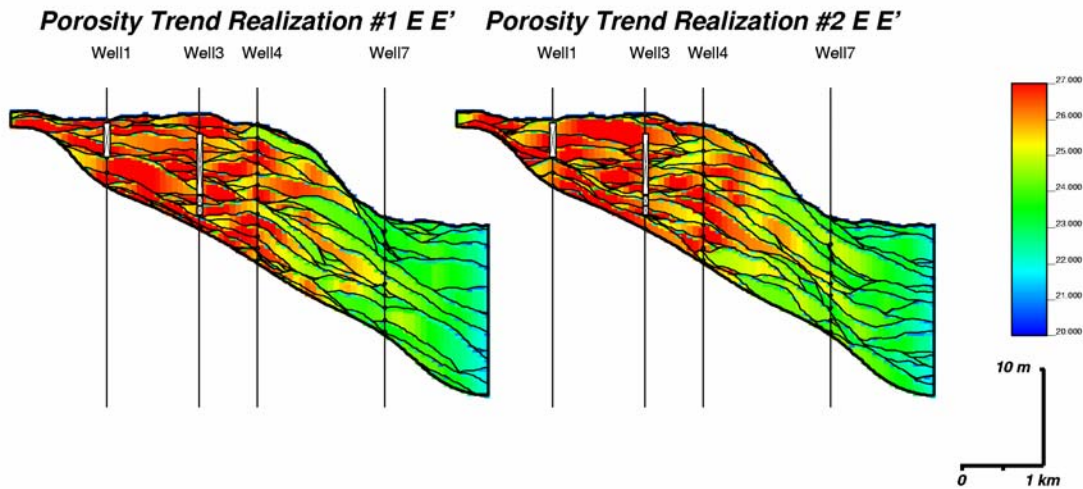
Figure 20 – porosity (percent) hierarchical trend models. The trends described in Figure 19 are reproduced and the trend model mean is corrected to the declustered mean from the well logs.
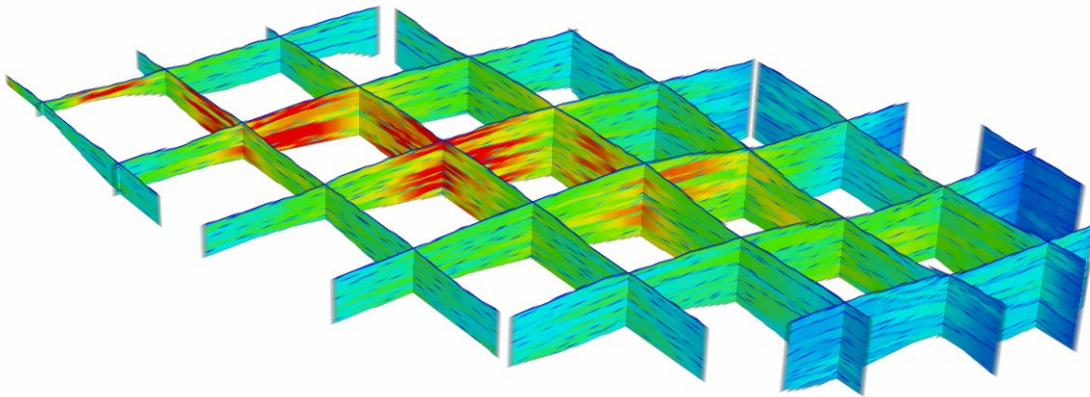
Figure 21 – fence diagram of the first realization of the porosity hierarchical trend model. (30 times vertical exaggeration). Color scale is the same as in Figure 20.
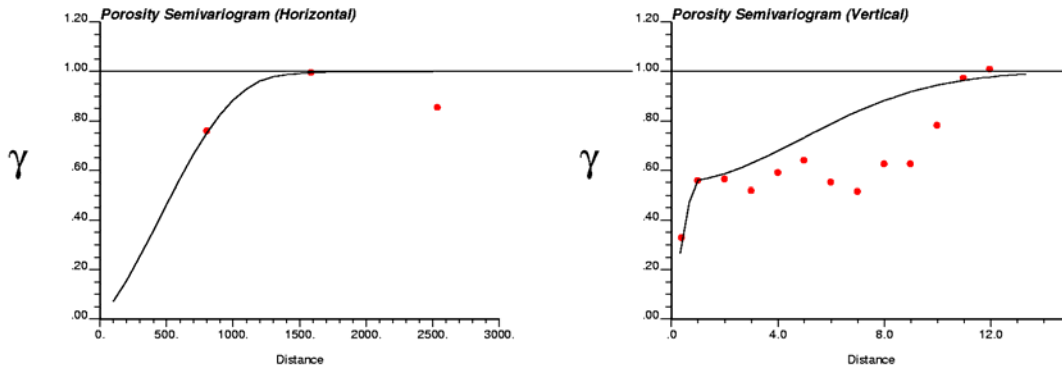
Figure 22 – Horizontal and vertical semivariograms of the Gaussian transform of the porosity well log data.
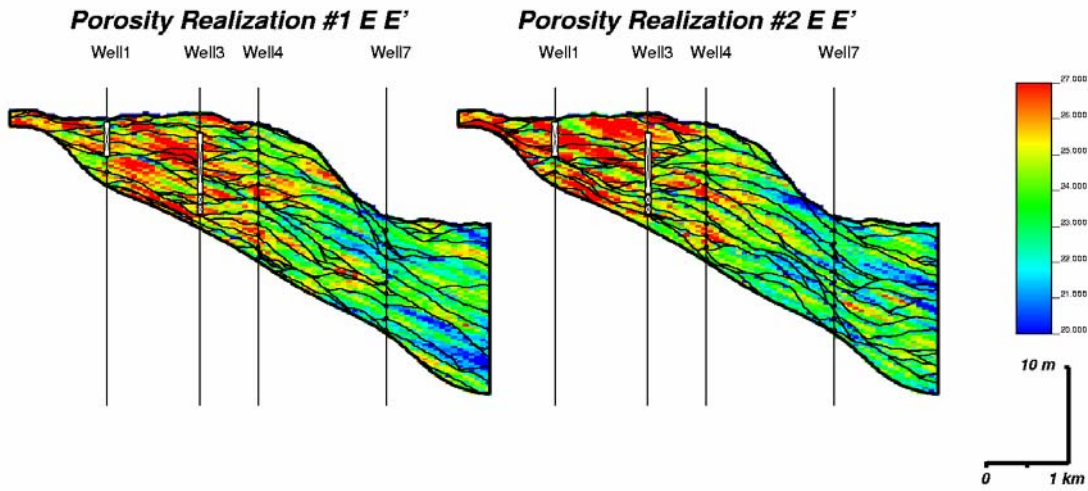

Figure 23 – Two realizations of porosity constrained to the surface based hierarchical trend model and conditioned to well logs.
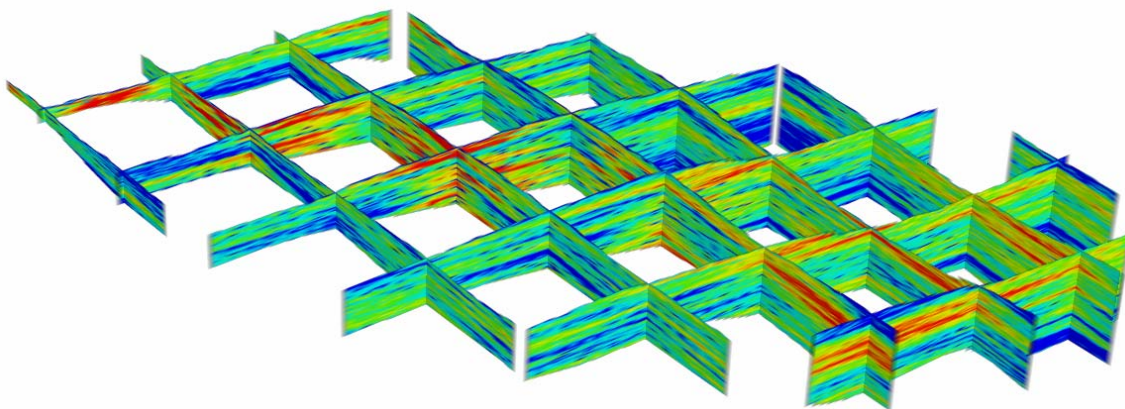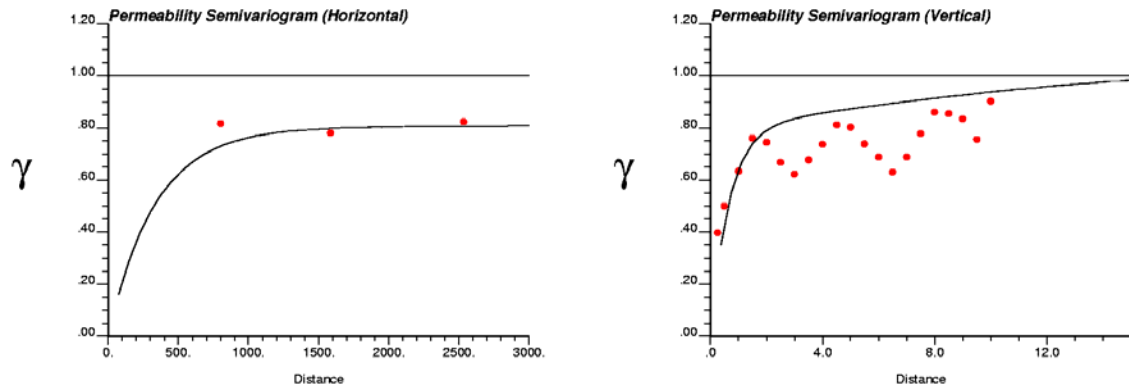

Figure 24 - fence diagram of the first porosity realization of the porosity hierarchical trend model (30 times vertical exaggeration). Color scale is the same as in Figure 20.

Figure 25 - Horizontal and vertical semivariograms of the Gaussian transform of the permeability well log data.
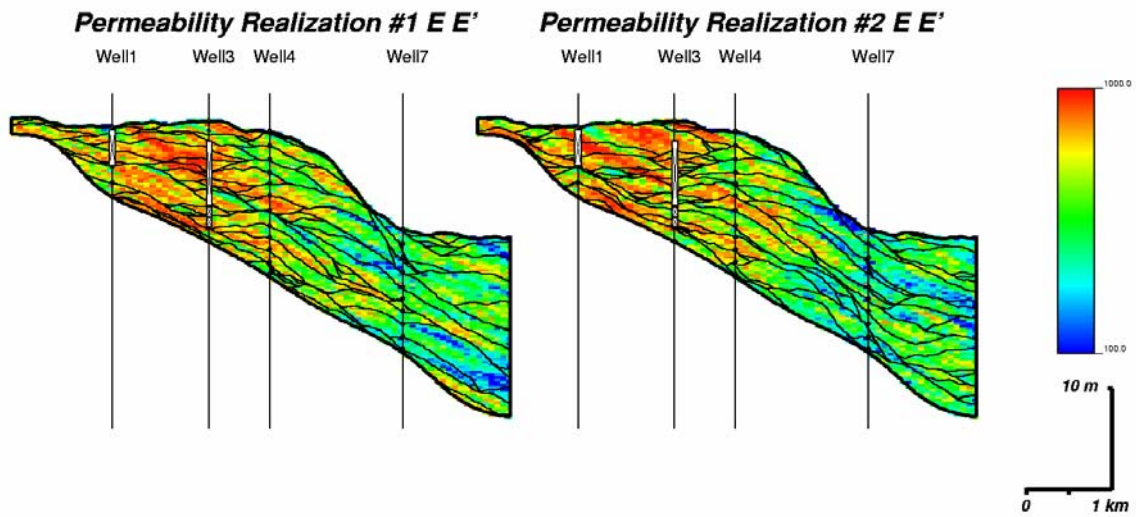

Figure 26 – Two realizations of permeability correlated to the paired porosity realizations and conditioned to well logs.
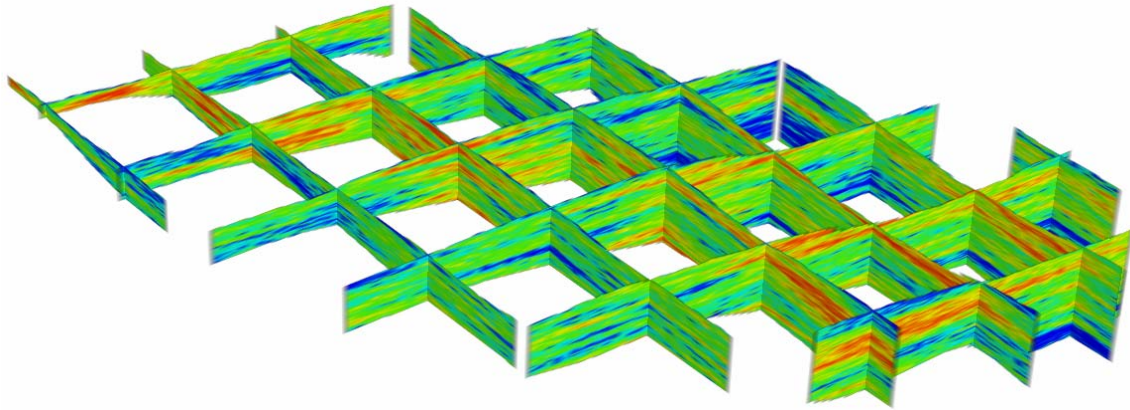
Figure 27 - fence diagram of the first permeability realization (30 times vertical exaggeration). Color scale is the same as in Figure 26.
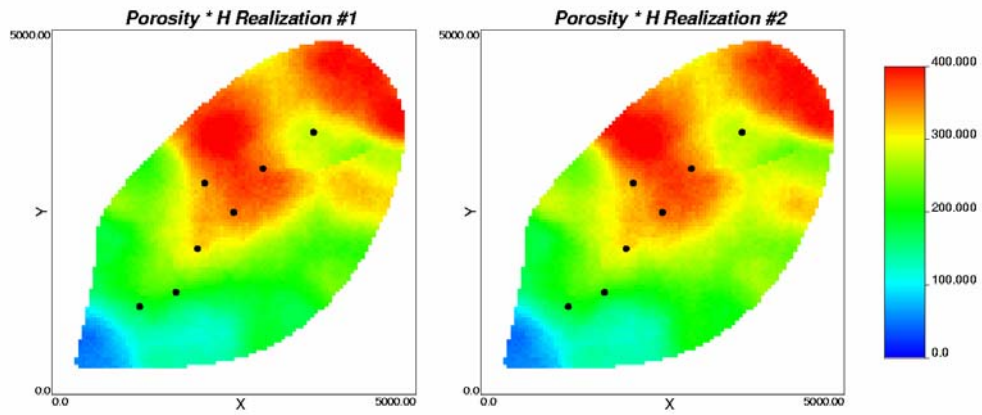

Figure 28 – φh maps for two realizations of porosity.